Mathematics

https://www.aimspress.com/journal/Math

AIMS Mathematics, 11(7): 23282–23307.
DOI: 10.3934/math.2026939
Received: 29 May 2026
Revised: 15 July 2026
Accepted: 24 July 2026
Published: 30 July 2026

Research article

Primary resonance and multi-strategy time-delayed feedback control for fractional-order economic fluctuation systems

Xiaorong Zhang[1], **Lihan Jia**[2], **and Zhoujin Cui**[2,*]

[1] School of Economics and Management, Jiangsu Maritime Institute, Nanjing, 211170, China
[2] School of Mathematical Sciences, Jiangsu Second Normal University, Nanjing, 210013, China

* **Correspondence:** Email: cuizhoujin@126.com.

Abstract: Fractional-order modeling has become a standard approach to characterize long-memory and hereditary behaviors in macroeconomic and financial fluctuation systems. This paper constructed a fractional-order Duffing-Holmes economic fluctuation model subjected to constant and periodic compound excitations. Constant excitation characterized long-term fiscal inertia and steady investment trends, whereas periodic excitation represented business cycles and seasonal economic shocks. The multiple scale method was adopted to derive the primary resonance amplitude-frequency relation. The influences of fractional order, damping, and stiffness parameters on resonant intensity and system stability were systematically examined. To suppress the excessive oscillation, jump, and hysteresis of economic cycles, four nonlinear time-delayed feedback schemes including displacement, velocity, acceleration, and hybrid velocity-acceleration feedback were proposed. Analytical amplitude-frequency solutions under each control strategy were derived. Numerical results from amplitude-frequency curves and time-domain trajectories demonstrated that all controllers can effectively reduce resonance magnitude and eliminate multivalued bifurcation. In particular, the hybrid feedback scheme exhibited the strongest suppression effect. The findings provided theoretical support and policy reference for countercyclical regulation of fractional-order macroeconomic fluctuation systems.

Keywords: fractional-order economic fluctuation system; primary resonance; Duffing-Holmes model; time-delayed feedback control; multiple scale method
Mathematics Subject Classification: 34E13, 34K35, 91B55

1. Introduction

Economic fluctuation and business cycle evolution have always been core topics in macroeconomics and nonlinear dynamics. Classical theories represented by Goodwin, Kaldor, and Kalecki established the basic framework for cyclic fluctuation, nonlinear investment behavior, and economic equilibrium evolution [1–4]. Subsequent studies further investigated limit cycle dynamics, equilibrium stability, and cyclical dynamics under investment lags and policy intervention. The surveys by Gabisch & Lorenz [5], Puu [6], together with the cubic-nonlinearity model of Puu & Sushko [7] , lay the groundwork for business cycle theory and nonlinear dynamics. Analyses by Takeuchi & Yamamura [8], Franke et al. [9], and Hartwig [10] discussed macroeconomic stability and growth from the perspectives of time delays, wage-price feedback and semi-endogenous growth. Nevertheless, traditional integer-order models are insufficient to describe the widespread long-memory, path dependence and policy transmission inertia observed in real economic operations.

With the advancement of fractional calculus, fractional-order differential equations become a credible modeling tool for complex economic systems [11, 12]. A representative work by Lin et al. [11] verifies that fractional derivatives can capture the memory hysteresis of economic variables that feature integer-order models fail to reproduce. Existing fractional financial and economic control studies can be divided into two categories. The first category only constructs open-loop fractional dynamic models without intervention feedback [13–15], which merely describe system inherent dynamics without regulation design. The second category adopts single control forms including parameter switching, projection synchronization, and sliding mode control as shown in [16–20]. Recent advances in fractional-order financial systems, such as the dynamics analysis of fractional-order chaotic econometric systems [12] and function projection synchronization for financial risk systems [20], have further enriched the understanding of complex behaviors. However, these studies, like the earlier works, still rely on single control strategies and do not systematically compare multi-feedback delayed control frameworks. Practically, real macroeconomic systems are jointly driven by two kinds of external shocks: Constant excitations from long-term fiscal rules and fixed baseline investment, and periodic excitations generated by business cycles and credit swings [21, 22]. The interaction between fractional memory effects and compound dual excitations readily induces primary resonance, which magnifies economic volatility and triggers state jumps and hysteresis bifurcation, posing clear threats to macro and financial stability.

Time delay is an inherent attribute of macro decision-making and policy implementation, mainly reflected in policy formulation, information transmission, and investment execution lags [23,24]. Time-delayed feedback control has been widely applied in nonlinear dynamic regulation, as it can naturally simulate the lag characteristics in actual economic policy formulation and implementation [25–28]. However, most existing literature only employs a single feedback form to suppress economic chaos and cyclic amplitude, lacking systematic comparison and inherent mechanism interpretation of multiple feedback strategies. More importantly, the economic connotation and differentiated regulatory logic of displacement, velocity, acceleration, and hybrid feedback remain underexamined in fractional economic fluctuation research.

Compared with the existing literature, the novelty of this work is threefold. First, unlike most previous studies that focus solely on open-loop fractional economic models without feedback intervention or adopt a single control form, this paper systematically designs and compares four distinct time-delayed feedback frameworks, including displacement, velocity, acceleration, and hybrid velocity-acceleration feedback. Second, while our previous work [29] investigated superharmonic resonance in the fractional Mathieu-Duffing equation, the present study addresses primary resonance under combined constant and periodic excitations, which is economically more relevant as it captures the simultaneous influence of long-term fiscal inertia and short-term business cycle shocks. Third, this paper provides explicit analytical amplitude-frequency relations for each control strategy and quantifies their suppression performance through unified metrics, offering a clear theoretical basis for policy selection in macroeconomic stabilization. Collectively, these three contributions form a systematic framework that integrates fractional-order modeling, resonance analysis, and multi-strategy delayed feedback control. This framework not only addresses the research gaps identified in existing literature but also provides a comprehensive theoretical foundation for designing and selecting appropriate countercyclical policies in fractional-order macroeconomic systems.

Motivated by the above research shortages, this paper establishes a fractional-order Duffing-Holmes model to characterize economic fluctuations under constant and periodic excitations. The multiple scale method is used to derive primary resonance amplitude-frequency responses. Parameter influences on resonant behaviors are analyzed. Four time-delayed feedback controllers are designed to suppress resonance, jump, and hysteresis. Numerical comparisons in both frequency and time domains verify control performance. The results offer theoretical basis and policy implications for macroeconomic dynamic analysis and countercyclical regulation.

2. Primary resonance

Based on the classical Goodwin-Kaldor economic fluctuation framework and existing fractional dynamic modeling ideas [3, 11, 30], this paper constructs a fractional-order nonlinear damped Duffing-Holmes dynamic equation to describe the evolution law of macroeconomic cycle fluctuation. The model incorporates economic long-memory, nonlinear investment-consumption behavior, and dual shocks from persistent policy trend and periodic cyclic oscillation. The governing equation reads:

$$\ddot{x} + \alpha\dot{x} + \beta\dot{x}^3 + \gamma x + \eta x^3 + \mu D_t^q x = f_0 + f_1 \cos\omega t, \tag{2.1}$$

where $x(t)$ denotes the output gap, i.e., the deviation of real economic output from its equilibrium steady state. The linear stiffness γ reflects intrinsic stabilization via automatic price and wage adjustments, while the cubic stiffness η captures nonlinear saturation triggered by resource constraints and inflation pressure during economic overheating. Linear damping α corresponds to spontaneous fluctuation dissipation through market clearing mechanisms, and nonlinear damping β measures amplitude-varying countercyclical adjustments in investment and consumption. The term $D_t^q x$ stands for the Caputo fractional derivative with order $0 < q \leq 1$, which characterizes long memory and path dependence embedded in economic policies and market expectations. Its formal definition reads

$$D_t^q x(t) = \frac{1}{\Gamma(1-q)} \int_0^t \dot{x}(\xi)\,(t-\xi)^{-q} \mathrm{d}\xi, \tag{2.2}$$

where $\Gamma(z)$ is the Euler gamma function satisfying the recursion $\Gamma(z+1) = z\Gamma(z)$. The coefficient μ quantifies the strength of this fractional long-memory effect.

For external forcing terms, the constant excitation f_0 stands for persistent fiscal inertia and baseline investment trends, whereas the periodic excitation $f_1 \cos\omega t$ describes business cycle and seasonal shocks. All simulation parameters take dimensionless values following widely accepted empirical calibration standards. He and Wang [31] fitted fractional orders between 0.7 and 0.95 with macroeconomic data from the U.S., Australia, and the United Kingdom, which justifies our choice of $q = 0.9$ for subsequent numerical analysis.

The established model well captures nonlinear evolution, memory dependence, and external shock response of real macro systems, and can reflect economic operation under combined market self-regulation and policy intervention. Primary resonance occurs when excitation frequency ω approaches the linear natural frequency $\omega_0 \overset{\text{def}}{=} \sqrt{\gamma}$. Economically, this corresponds to the resonance between policy cycle and inherent economic cycle, which amplifies cyclic volatility and induces complex dynamic responses such as jump and hysteresis.

2.1. Amplitude-frequency response equation

This section employs the multiple scale method to solve the primary resonance responses of Eq (2.1). As a classic perturbation technique well-suited for resonant and time-delay systems featuring multi-time-scale properties [32–34], it outperforms the averaging method and iterative perturbation schemes. The multiple scale framework cleanly decouples fast oscillating and slowly evolving time variables, enabling accurate derivation of closed-form amplitude-frequency relations for fractional systems driven by combined constant and periodic excitations. For this process, a small perturbation parameter ε is introduced to separate different time scales $T_n = \varepsilon^n t, (n = 0, 1)$, then an approximate solution of Eq (2.1) with small amplitudes can be represented by

$$x = x_0(T_0, T_1) + \varepsilon x_1(T_0, T_1) + \cdots \tag{2.3}$$

To ensure weak damping and weak nonlinearity, the fractional and nonlinear terms are scaled by the small parameter ε as follows,

$$\alpha \to \varepsilon\alpha, \quad \beta \to \varepsilon\beta, \quad \eta \to \varepsilon\eta, \quad \mu \to \varepsilon\mu, \quad f_1 \to \varepsilon f_1. \tag{2.4}$$

Then, Eq (2.1) becomes

$$\ddot{x} + \omega_0^2 x + \varepsilon\alpha\dot{x} + \varepsilon\beta\dot{x}^3 + \varepsilon\eta x^3 + \varepsilon\mu D_t^q x = f_0 + \varepsilon f_1 \cos\omega t, \tag{2.5}$$

in which $\omega_0 = \sqrt{\gamma}$ is the undamped natural frequency of the system.

The derivatives with respect to t can be expressed in terms of the new scaled times T_n as a series of partial derivatives

$$\frac{\mathrm{d}}{\mathrm{d}t} = \frac{\partial}{\partial T_0}\frac{\mathrm{d}T_0}{\mathrm{d}t} + \frac{\partial}{\partial T_1}\frac{\mathrm{d}T_1}{\mathrm{d}t} + \cdots = D_0 + \varepsilon D_1 + \cdots, \tag{2.6a}$$

$$\frac{\mathrm{d}^2}{\mathrm{d}t^2} = D_0^2 + 2\varepsilon D_0 D_1 + \varepsilon^2 D_1^2 + \cdots, \tag{2.6b}$$

$$D_t^q = D_0^q + q\varepsilon D_0^{q-1} D_1 + \cdots, \tag{2.6c}$$

in which $D_0^q = \frac{\partial^q}{\partial T_0^q}$, $D_n = \frac{\partial}{\partial T_n}$, $D_n^2 = \frac{\partial^2}{\partial T_n^2}$, $(n = 0, 1)$.

The resonance relation is considered as $\omega = \omega_0$ or $\omega \approx \omega_0$, and a detuning parameter σ describing the nearness of ω to ω_0 is introduced by

$$\omega = \omega_0 + \varepsilon\sigma, \tag{2.7}$$

then $\omega t = \omega_0 T_0 + \sigma T_1$. Substituting (2.3), (2.6b), and (2.6c) into (2.5) leads to the following equation

$$\begin{aligned}&(D_0^2 + 2\varepsilon D_0 D_1 + \varepsilon^2 D_1^2)(x_0 + \varepsilon x_1) + \omega_0^2(x_0 + \varepsilon x_1) + \varepsilon\mu \cdot (D_0^q + q\varepsilon D_0^{q-1} D_1)(x_0 + \varepsilon x_1)\\&+ \varepsilon\alpha \cdot (D_0 + \varepsilon D_1)(x_0 + \varepsilon x_1) + \varepsilon\beta \cdot [(D_0 + \varepsilon D_1)(x_0 + \varepsilon x_1)]^3 + \varepsilon\eta \cdot (x_0 + \varepsilon x_1)^3\\&= f_0 + \varepsilon f_1 \cos(\omega T_0 + \sigma T_1).\end{aligned}$$

Equating the coefficients of the same power of ε, a set of linear differential equations is obtained:

$$O(\varepsilon^0) : D_0^2 x_0 + \omega_0^2 x_0 = f_0, \tag{2.8}$$

$$\begin{aligned}O(\varepsilon^1) : D_0^2 x_1 + \omega_0^2 x_1 = &- 2D_0 D_1 x_0 - \mu D_0^q x_0 - \alpha D_0 x_0 - \beta(D_0 x_0)^3 - \eta x_0^3\\&+ f_1 \cos(\omega T_0 + \sigma T_1),\end{aligned} \tag{2.9}$$

from which x_0 and x_1 can be solved sequentially. In this way, the resonant solution x is dominated by x_0, collected by εx_1.

The general solution of Eq (2.8) is of the form

$$x_0 = A(T_1)\mathrm{e}^{\mathrm{i}\omega_0 T_0} + \overline{A}(T_1)\mathrm{e}^{-\mathrm{i}\omega_0 T_0} + \Lambda, \tag{2.10}$$

where $A(T_1)$ and $\overline{A}(T_1)$ are unknown functions, and $\overline{A}(T_1)$ denotes the complex conjugate of $A(T_1)$, $\Lambda = \frac{f_0}{\omega_0^2}$.

To proceed with the solution of Eq (2.9), we first derive the Caputo fractional derivative of the harmonic function $\mathrm{e}^{\mathrm{i}\omega t}$ for $0 < q \leq 1$. Substituting $x(t) = \mathrm{e}^{\mathrm{i}\omega t}$ into (2.2), the first-order derivative reads $\dot{x}(t) = \mathrm{i}\omega\mathrm{e}^{\mathrm{i}\omega t}$, which yields

$$D_t^q \mathrm{e}^{\mathrm{i}\omega t} = \frac{1}{\Gamma(1-q)} \int_0^t \mathrm{i}\omega\mathrm{e}^{\mathrm{i}\omega\xi}(t-\xi)^{-q}\mathrm{d}\xi. \tag{2.11}$$

Implement variable substitution $s = t - \xi$, namely, $\xi = t - s$ and $\mathrm{d}\xi = -\mathrm{d}s$. Rearranging (2.11) yields

$$D_t^q \mathrm{e}^{\mathrm{i}\omega t} = \frac{\mathrm{i}\omega\mathrm{e}^{\mathrm{i}\omega t}}{\Gamma(1-q)} \int_0^t \mathrm{e}^{-\mathrm{i}\omega s} s^{-q}\mathrm{d}s. \tag{2.12}$$

For steady-state periodic primary resonance, the transient integral from finite upper limit t can be neglected, and we extend the integral upper limit to positive infinity. This treatment constitutes the steady-state approximation for long-term periodic motion. We introduce the standard gamma integral identity

$$\int_0^{+\infty} \mathrm{e}^{-ks} s^{z-1}\mathrm{d}s = \Gamma(z)k^{-z}. \tag{2.13}$$

Set $k = \mathrm{i}\omega$, $z = 1 - q$. The infinite integral term of (2.13) is simplified as

$$\int_0^{+\infty} \mathrm{e}^{-\mathrm{i}\omega s} s^{-q}\mathrm{d}s = \Gamma(1-q)(\mathrm{i}\omega)^{q-1}. \tag{2.14}$$

Substitute the simplified infinite integral (2.14) back into the fractional derivative expression and perform algebraic simplification:

$$D_t^q \mathrm{e}^{\mathrm{i}\omega t} \approx \frac{\mathrm{i}\omega\mathrm{e}^{\mathrm{i}\omega t}}{\Gamma(1-q)} \cdot \Gamma(1-q)(\mathrm{i}\omega)^{q-1} = (\mathrm{i}\omega)^q \mathrm{e}^{\mathrm{i}\omega t}. \tag{2.15}$$

The equality holds exactly for the infinite integral, whereas the expression serves as an approximation for finite t in steady periodic resonance.

Remark 1. To focus on long-term steady primary resonance dynamics, the fractional integral's upper bound is extended to infinity; finite-time transient terms decay in power-law form and can be discarded when solving steady-state responses. This standard multiple-scales simplification for fractional oscillators is commonly adopted to obtain closed-form amplitude-frequency relations [11, 29]. Rigorous justification is provided by analyzing the integral's asymptotic behavior as $t \to \infty$, which verifies that the semi-infinite integral dominates the total integral contribution.

Substituting (2.10) and (2.15) into Eq (2.9), by the fact that the fractional derivative of a constant is zero under the Caputo definition and using

$$\cos(\omega_0 T_0 + \sigma T_1) = \frac{e^{i(\omega_0 T_0+\sigma T_1)} + e^{-i(\omega_0 T_0+\sigma T_1)}}{2},$$

the righthand of Eq (2.9) becomes

$$[-2i\omega_0 D_1 A - \mu A(i\omega_0)^q - i\omega_0\alpha A - 3\beta i\omega_0^3 A^2\bar{A} - 3\eta A^2\bar{A} - 3\eta\Lambda^2 A + \frac{f_1}{2}e^{i\sigma T_1}]e^{i\omega_0 T_0} + NST + cc, \quad (2.16)$$

where NST stands for the terms that do not produce secular terms, and cc denotes the complex conjugate of the preceding terms.

In order that x_1 is periodic, the secular terms with $e^{i\omega_0 T_0}$ must be zero, namely,

$$2i\omega_0 D_1 A + \mu A(i\omega_0)^q + i\omega_0\alpha A + 3\beta i\omega_0^3 A^2\bar{A} + 3\eta A^2\bar{A} + 3\eta\Lambda^2 A - \frac{f_1}{2}e^{i\sigma T_1} = 0. \quad (2.17)$$

With the help of the Euler formula

$$i^q = (e^{i\pi/2})^q = e^{iq\pi/2} = \cos\frac{q\pi}{2} + i\sin\frac{q\pi}{2}, \quad (2.18)$$

let $\varphi \overset{\text{def}}{=} \sigma T_1 - \theta$. By separating the real and imaginary parts of Eq (2.17), the differential equations governing amplitude $a(T_1)$ and $\varphi(T_1)$ of $A(T_1)$ are expressed respectively as follows

$$D_1 a = -\frac{\mu a}{2}\omega_0^{q-1}\sin\frac{q\pi}{2} - \frac{\alpha a}{2} - \frac{3\beta a^3}{8}\omega_0^2 + \frac{f_1}{2\omega_0}\sin\varphi, \quad (2.19a)$$

$$aD_1\varphi = \sigma a - \frac{\mu a}{2}\omega_0^{q-1}\cos\frac{q\pi}{2} - \frac{3\eta\Lambda^2}{2\omega_0}a - \frac{3\eta}{8\omega_0}a^3 + \frac{f_1}{2\omega_0}\cos\varphi. \quad (2.19b)$$

The steady-state motions for the primary resonance response correspond to the fixed points of (2.19a) and (2.19b), that is, $D_1 a = 0$ and $D_1\varphi = 0$, namely,

$$-\frac{\mu a}{2}\omega_0^{q-1}\sin\frac{q\pi}{2} - \frac{\alpha a}{2} - \frac{3\beta a^3}{8}\omega_0^2 = -\frac{f_1}{2\omega_0}\sin\varphi, \quad (2.20a)$$

$$\sigma a - \frac{\mu a}{2}\omega_0^{q-1}\cos\frac{q\pi}{2} - \frac{3\eta\Lambda^2}{2\omega_0}a - \frac{3\eta}{8\omega_0}a^3 = -\frac{f_1}{2\omega_0}\cos\varphi. \quad (2.20b)$$

By performing square operations and eliminating φ from Eqs (2.20a) and (2.20b), the following amplitude-frequency response equation is determined,

$$[(\frac{\mu}{2}\omega_0^{q-1}\sin\frac{q\pi}{2}+\frac{\alpha}{2}+\frac{3\beta\omega_0^2}{8}a^2)^2+(\sigma-\frac{\mu}{2}\omega_0^{q-1}\cos\frac{q\pi}{2}-\frac{3\eta\Lambda^2}{2\omega_0}-\frac{3\eta}{8\omega_0}a^2)^2]a^2=(\frac{f_1}{2\omega_0})^2. \tag{2.21}$$

Equation (2.21) reveals that the resonance amplitude depends on the excitation magnitude, while being modulated by the combined effects of fractional damping, nonlinear stiffness, and time-delayed feedback control parameters.

2.2. Stability, equilibrium classification, and saddle-node bifurcation analysis

2.2.1. Linearization and local stability criterion

To judge the stability and type of steady resonant equilibria, we linearize the amplitude-phase evolution equations around a fixed solution. Let (a^*,φ^*) denote a steady equilibrium of Eqs (2.19a) and (2.19b), and define the small perturbations $\Delta a = a - a^*$, $\Delta\varphi = \varphi - \varphi^*$. The linearized governing system for perturbations reads

$$D_1\Delta a = -\left[\frac{\mu}{2}\omega_0^{q-1}\sin\frac{q\pi}{2}+\frac{\alpha}{2}+\frac{9\beta(a^*)^2}{8}\omega_0^2\right]\Delta a+\frac{f_1}{2\omega_0}\cos\varphi^*\,\Delta\varphi, \tag{2.22a}$$

$$D_1\Delta\varphi = \left[\frac{\sigma}{a^*}-\frac{\mu}{2a^*}\omega_0^{q-1}\cos\frac{q\pi}{2}-\frac{3\eta\Lambda^2}{2\omega_0a^*}-\frac{9\alpha}{8\omega_0}a^*\right]\Delta a-\frac{f_1}{2\omega_0a^*}\sin\varphi^*\,\Delta\varphi. \tag{2.22b}$$

We introduce the lumped coefficients

$$P=\frac{\mu}{2}\omega_0^{q-1}\sin\frac{q\pi}{2}+\frac{\alpha}{2}+\frac{9\beta(a^*)^2}{8}\omega_0^2,\quad Q=\frac{\mu}{2}\omega_0^{q-1}\sin\frac{q\pi}{2}+\frac{\alpha}{2}+\frac{3\beta(a^*)^2}{8}\omega_0^2,$$
$$M=\sigma-\frac{\mu}{2}\omega_0^{q-1}\cos\frac{q\pi}{2}-\frac{3\eta\Lambda^2}{2\omega_0}-\frac{3\eta}{8\omega_0}(a^*)^2,\quad N=\sigma-\frac{\mu}{2}\omega_0^{q-1}\cos\frac{q\pi}{2}-\frac{3\eta\Lambda^2}{2\omega_0}-\frac{9\alpha}{8\omega_0}(a^*)^2,$$

then the characteristic equation from the perturbation matrix takes the form

$$\begin{vmatrix} -P-\lambda & -a^*M \\ \frac{1}{a^*}N & -Q-\lambda \end{vmatrix}=0. \tag{2.23}$$

Expanding the determinant yields

$$\lambda^2+(P+Q)\lambda+(PQ+MN)=0. \tag{2.24}$$

Define $m=P+Q$, $n=PQ+MN$, and rewrite the characteristic polynomial as

$$\lambda^2+m\lambda+n=0. \tag{2.25}$$

By the Routh-Hurwitz criterion, the equilibrium (a^*,φ^*) is asymptotically stable if, and only if,

$$m>0,\quad n>0. \tag{2.26}$$

Equilibrium types are classified based on the discriminant $\Delta=m^2-4n$ together with the signs of m and n:

- Stable node: $\Delta > 0$, $m > 0$, $n > 0$ (two distinct negative real eigenvalues);
- Unstable node: $\Delta > 0$, $m < 0$, $n > 0$ (two distinct positive real eigenvalues);
- Saddle point: $n < 0$ (real eigenvalues with opposite signs);
- Stable focus: $\Delta < 0$, $m > 0$ (complex conjugate eigenvalues with negative real parts);
- Unstable focus: $\Delta < 0$, $m < 0$ (complex conjugate eigenvalues with positive real parts);
- Center: $\Delta < 0$, $m = 0$, $n > 0$ (purely imaginary conjugate eigenvalues).

2.2.2. Numerical illustration of local stability

We present a numerical example to verify the above stability analysis for fractional Duffing-Holmes economic oscillators. All simulated parameters are dimensionless and selected following standard calibration rules from fractional macroeconomic dynamics literature. The fractional order $q \in (0.6, 1]$ is adopted to capture the strong long-memory persistence of aggregate economic variables, as validated in Lin et al. [11] and fractional business-cycle models in [16]. Damping and stiffness parameters $\alpha = 0.03$, $\mu = 0.02$, $\eta = 0.25$ fall within typical ranges for qualitative resonance analysis [11, 31, 35]. Excitation magnitudes $f_0 = 0.2$, $f_1 = 0.1$ retain the weakly nonlinear assumption required by the multiple-scale perturbation method. These values are not calibrated against real macroeconomic time series but form a representative parameter space for theoretical analysis of resonance and control effects. This paper focuses on revealing intrinsic resonance suppression mechanisms rather than providing quantitative economic forecasts.

Adopt the baseline parameter group $q = 0.9, \alpha = 0.03, \beta = 0.02, \eta = 0.25, \mu = 0.02, f_0 = 0.2, f_1 = 0.1, \omega_0 = 1.0, \sigma = 0.01$. Solving Eq. (2.21) gives the steady amplitude $a^* \approx 0.458$. Substitute this equilibrium to compute $P \approx 0.0182$, $Q \approx 0.0161$, $M \approx -0.0235$, $N \approx -0.0458$, which further yield $m = P + Q \approx 0.0343 > 0$ and $n = PQ + MN \approx 0.00083 > 0$. The Routh-Hurwitz conditions are satisfied, confirming asymptotic stability. The discriminant $\Delta = m^2 - 4n \approx -0.0032 < 0$ indicates a pair of complex conjugate eigenvalues with negative real parts, so this equilibrium corresponds to a stable focus. The numerical test validates the reliability of the proposed stability framework, and implies that reasonable policy tuning can stabilize the economy near equilibrium and suppress violent cyclical swings.

2.2.3. Saddle-node bifurcation critical condition and economic implication

The above local stability analysis only describes dynamic behavior around a single equilibrium. To identify parameter thresholds triggering volatile economic fluctuations, we derive the saddle-node bifurcation boundary. Saddle-node bifurcation occurs at $n = 0$, the critical condition where two equilibria collide and disappear. Substitute the definitions of P, Q, M, N into $n = PQ + MN = 0$ to obtain the implicit bifurcation constraint

$$\begin{aligned}&\left[\frac{\mu}{2}\omega_0^{q-1}\sin\frac{q\pi}{2}+\frac{\alpha}{2}+\frac{9\beta(a^*)^2}{8}\omega_0^2\right]\left[\frac{\mu}{2}\omega_0^{q-1}\sin\frac{q\pi}{2}+\frac{\alpha}{2}+\frac{3\beta(a^*)^2}{8}\omega_0^2\right]\\&+\left[\sigma-\frac{\mu}{2}\omega_0^{q-1}\cos\frac{q\pi}{2}-\frac{3\eta\Lambda^2}{2\omega_0}-\frac{3\eta(a^*)^2}{8\omega_0}\right]\left[\sigma-\frac{\mu}{2}\omega_0^{q-1}\cos\frac{q\pi}{2}-\frac{3\eta\Lambda^2}{2\omega_0}-\frac{9\alpha(a^*)^2}{8\omega_0}\right]=0.\end{aligned} \tag{2.27}$$

Fix all baseline parameters and substitute $a^* \approx 0.458$ into Eq (2.27), where solving yields the critical fractional order $q_{cr} \approx 0.64$. If $q < q_{cr}$, we get $n < 0$ and the equilibrium degenerates to a saddle point;

minor periodic shocks will trigger sharp boom-bust jumps and persistent hysteresis loops of output gap. If $q > q_{\rm cr}$, $n > 0$ always holds, guaranteeing a unique stable resonant response without multivalued branches.

Equation (2.21) can be compactly rewritten as the implicit amplitude-frequency relation $F(a, \sigma) = 0$. Saddle-node bifurcation corresponds to double roots of $F(a, \sigma)$ with respect to a, satisfying the tangency condition $\partial F/\partial a = 0$. For fixed system parameters, this relation solves the critical detuning $\sigma_{\rm SN}$ and associated amplitude $a_{\rm SN}$. Using the same numerical parameters, the bifurcation point is $\sigma_{\rm SN} \approx 0.023$, $a_{\rm SN} \approx 0.52$. When $|\sigma| > |\sigma_{\rm SN}|$, only one stable equilibrium exists; when $|\sigma| < |\sigma_{\rm SN}|$, three equilibria coexist, which creates multivalued resonance curves and gives rise to jump and hysteresis phenomena.

This coexistence of multiple steady amplitudes under a single detuning value carries clear macroeconomic interpretations. Under identical policy frameworks and external shocks, the economy can settle at different output gap amplitudes solely due to differences in initial states and historical evolution paths. Mathematically, this solution multiplicity is the root of abrupt jump behavior: Minor continuous adjustments to the policy cycle, such as gradual shifts in fiscal stance, will induce discontinuous jumps in output amplitude once the system crosses the saddle-node threshold. Furthermore, the system features strong path dependence: The critical frequency triggering jumps differs depending on whether excitation frequency increases or decreases, which forms closed hysteresis loops. Economically, hysteresis implies that once severe cyclical volatility occurs, the economy fails to revert to mild low-amplitude fluctuations even if policy cycles return to their original settings, which constitutes a well-documented difficulty for real-world macroeconomic stabilization.

2.3. Parametric effects on primary resonance

The influence of different parameters on the amplitude of resonance solution is investigated numerically, as shown in the Figures 1 and 2, which presents parameter effect on the primary resonance amplitudes with respect to q, f_1, μ, η, α, and β. Here, the natural frequency is $\omega_0 = 1$. The parametric trends in Figure 1 validate the analytical predictions from Eq (2.21). In Figure 1(a), as the fractional-order q decreases, the amplitude of the response curve shows an increasing trend. Conversely, Figure 1(b) shows a different trend. As the amplitude of the harmonic excitation f_1 decreases, the amplitude of the response curve decreases as well. The phenomenon in Figure 1 illustrates that both the fractional-order and the amplitude of the harmonic excitation are key parameters that can alter the system's amplitude-frequency response characteristics in distinct ways. From an economic perspective, a smaller fractional order corresponds to stronger long-memory persistence of economic variables, which magnifies cyclic fluctuations and widens the deviation from economic equilibrium. Meanwhile, a larger periodic external shock inevitably intensifies business cycle volatility and expands the fluctuation range.

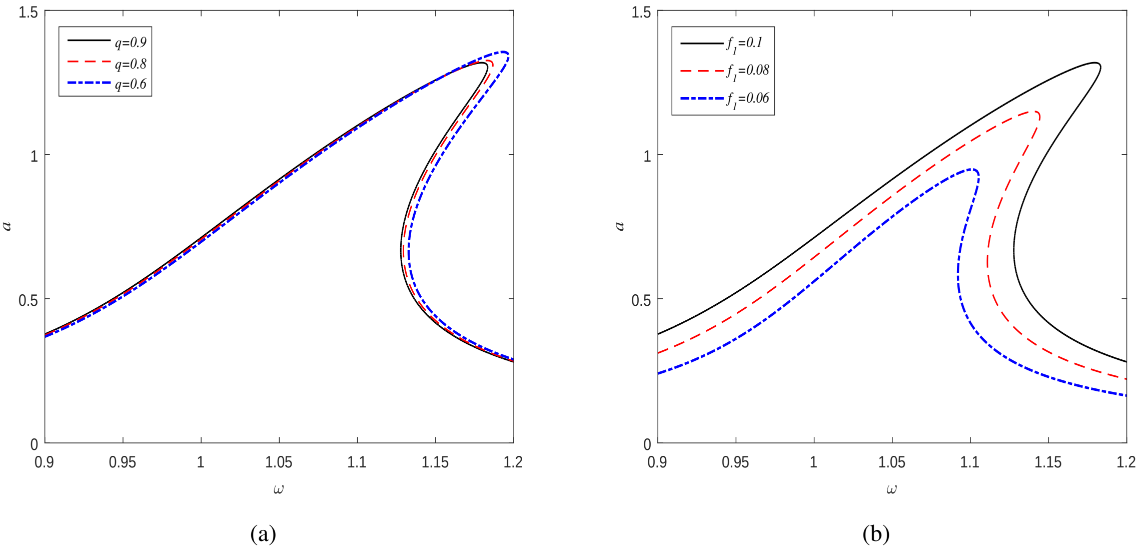

Figure 1. Parameter effect on the amplitude-frequency curves when (a) $\alpha = 0.03$, $\beta = 0.02$, $\eta = 0.25$, $\mu = 0.02$, $f_0 = 0.2$, $f_1 = 0.1$, (b) $q = 0.9$, $\alpha = 0.03$, $\beta = 0.02$, $\eta = 0.25$, $\mu = 0.02$, $f_0 = 0.2$.

In Figure 2(a), the primary resonance amplitude declines as the fractional damping coefficient μ rises. Larger fractional damping strengthens the system's intrinsic dissipation, thereby effectively restraining the resonant oscillation level at the natural frequency. As shown in Figure 2(b), the cubic stiffness coefficient η mainly shifts the overall amplitude-frequency curve toward higher frequencies, while barely changing the resonance peak magnitude. This suggests that nonlinear stiffness predominantly regulates the cyclic rhythm of the economic system, rather than altering the intensity of fluctuation amplitude. From Figure 2(c), a smaller linear viscous damping α corresponds to higher resonance amplitude. Lower linear energy dissipation weakens the system's self-stabilizing ability, making economic cycles more prone to intense oscillation. Meanwhile, Figure 2(d) shows that the growth of nonlinear damping coefficient β suppresses resonance amplitude obviously. Since nonlinear damping is amplitude-dependent, it exerts a stronger restraining effect on excessive volatility as oscillation intensity increases, which helps curb overheated economic fluctuation.

2.4. Verification of analytical solution by numerical integration

Finally, this section provides a numerical validation to compare the approximate analytical solution and the numerical solution. According to Eq (2.21), the primary resonance amplitude-frequency response curve of the system can be drawn. For comparison, this paper adopts the power series method introduced in reference [36, 37], and its calculation formula is

$$D_{t_n}^q[y(t_n)] \approx h^{-q} \sum_{j=0}^{n} C_j^q y(t_{n-j}), \tag{2.28}$$

where $t_n = nh$ are the sample points, h is the sample step, and C_j^q is the fractional binomial coefficient with the iterative relationship

$$C_0^q = 1, \quad C_j^q = (1 - \frac{1+q}{j})C_{j-1}^q. \tag{2.29}$$

According to Eqs (2.28) and (2.29), the numerical scheme for Eq (2.5) can be expressed as

$$x(t_n) = y(t_{n-1})h - \sum_{j=1}^{n} C_j^1 x(t_{n-j}), \tag{2.30a}$$

$$y(t_n) = [f_0 + f_1 \cos(\omega t_n) - \alpha y(t_{n-1}) - \beta y^3(t_{n-1}) - \gamma x(t_n) - \eta x^3(t_n) - \mu z(t_{n-1})]h - \sum_{j=1}^{n} C_j^1 y(t_{n-j}), \tag{2.30b}$$

$$z(t_n) = y(t_n)h^{1-q} - \sum_{j=1}^{n} C_j^{1-q} z(t_{n-j}). \tag{2.30c}$$

The sample step is set as $h = 0.005$, and the total computation time is 150 s. After omitting the temporary response in frontal 60 s, the peak value of the posterior response is taken as the steady-state amplitude by the numerical results.

Based on Eq (2.21), the amplitude-frequency response curve can be obtained analytically, as shown in Figure 3. According to Eqs (2.30a)–(2.30c), the amplitude-frequency response can be obtained by numerical integration, which is also shown in Figure 3 and represented by a circle. The parameters are as follows, $q = 0.82$, $\mu = 0.02$, $\alpha = 0.03$, $\beta = 0.02$, $\eta = 0.01$, $f_0 = 0.02$, and $f_1 = 0.06$. It can be seen from the observation in Figure 3 that the approximate analytical solution is in good agreement with the numerical results. It verifies that the multiple scale method is reliable for analyzing the resonance law of economic fluctuation systems and can provide effective theoretical support for economic cycle prediction.

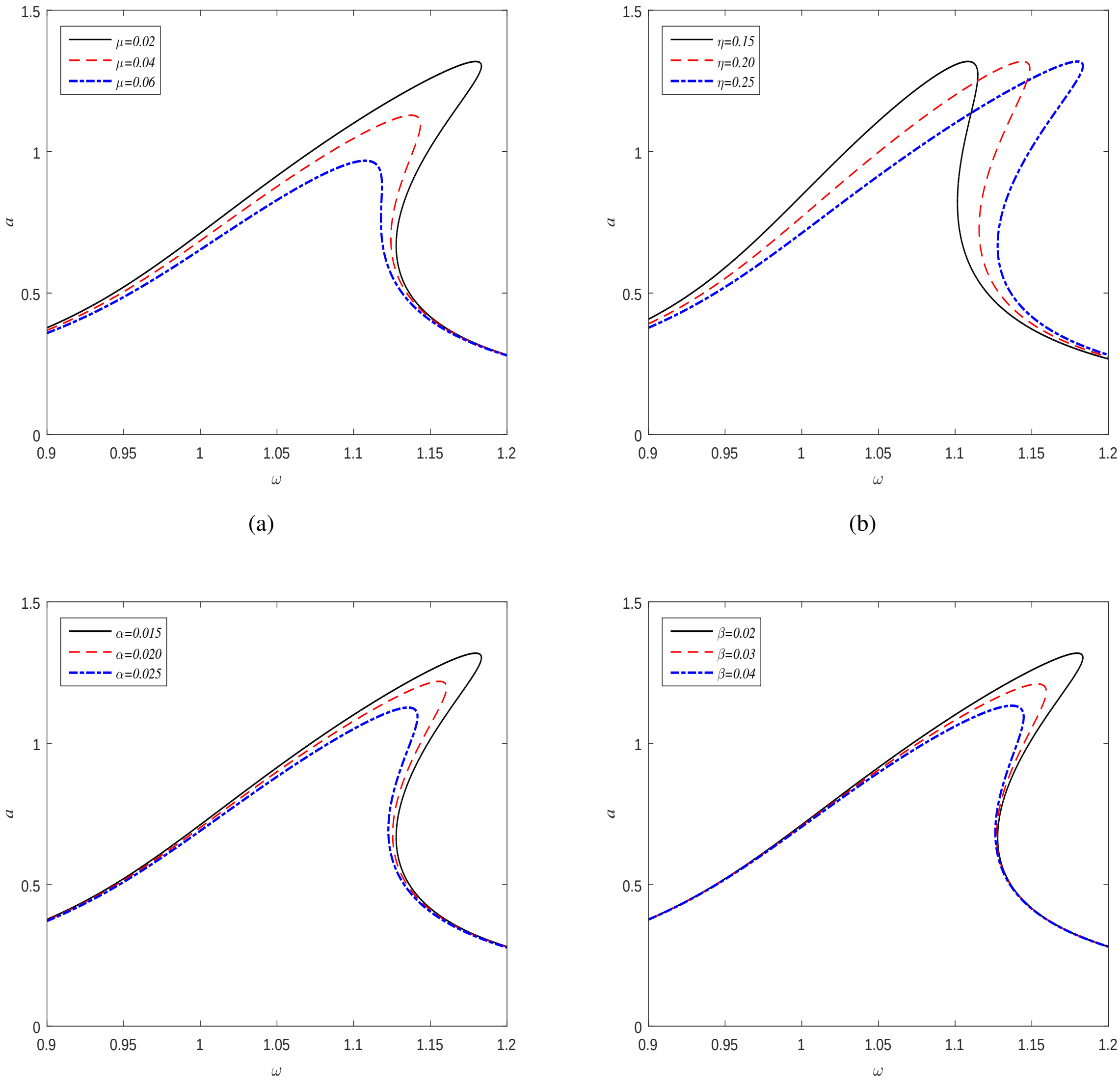

(a) (b) (c) (d)

Figure 2. Parameter effect on the amplitude-frequency curves when (a) q=0.9, $\alpha = 0.03$, $\beta = 0.02$, $\eta = 0.25$, $f_0 = 0.2$, $f_1 = 0.1$, (b) q=0.9, $\mu = 0.02$, $\alpha = 0.03$, $\beta = 0.02$, $f_0 = 0.2$, $f_1 = 0.1$, (c) q=0.9, $\mu = 0.02$, $\eta = 0.25$, $\beta = 0.02$, $f_0 = 0.2$, $f_1 = 0.1$, (d) q=0.9, $\mu = 0.02$, $\eta = 0.25$, $\alpha = 0.03$, $f_0 = 0.2$, $f_1 = 0.1$.

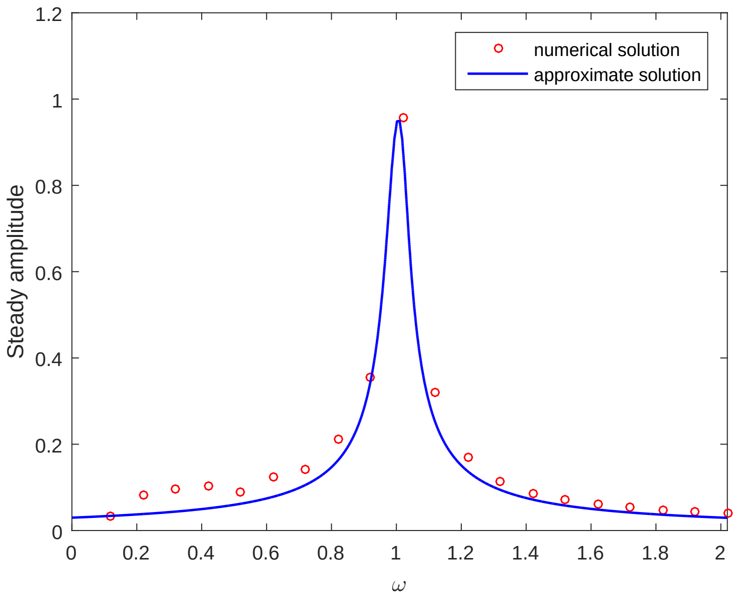

Figure 3. Comparison between approximate analytical solution and numerical solution.

3. Time-delayed feedback control and primary resonance regulation

3.1. Time-delayed feedback control strategies

To mitigate the adverse effects of primary resonance, such as amplitude mutation, jump behavior and hysteresis bifurcation on economic cyclic stability, this paper introduces nonlinear time-delayed feedback regulation as an effective suppression method. Considering the widespread policy decision lag, information transmission delay, and investment implementation lag in actual macroeconomic operations, time-delay control can well reflect the time-lag attribute of real countercyclical policy formulation and implementation. To clarify the regulatory mechanism and comparative suppression performance of different control schemes, the typical cubic time-delayed feedback strategies are established in this section, namely, displacement-based, velocity-based, and acceleration-based feedback, which take the following forms:

$$x^3(t-\tau),\quad \dot{x}^3(t-\tau)\ \text{ and }\ \ddot{x}^3(t-\tau).$$

Cubic feedback is adopted for three reasons. First, it conforms to the inherent cubic nonlinear terms ηx^3 and $\beta \dot{x}^3$ of the system, which facilitates consistent perturbation analysis. Second, cubic feedback retains structural symmetry: it imposes weak corrections for minor deviations and strong regulation for large deviations, consistent with real countercyclical policy rules. Third, linear feedback delivers limited suppression for large-amplitude oscillations, whereas quadratic feedback generates asymmetric control effects that shift equilibrium points and reshape stability boundaries. Further research will examine these alternative feedback structures in follow-up work.

3.1.1. Displacement feedback control

The fractional economic fluctuation dynamical model with displacement time-delayed feedback control can be established as follows:

$$\ddot{x} + \omega_0^2 x + \varepsilon\alpha\dot{x} + \varepsilon\beta\dot{x}^3 + \varepsilon\eta x^3 + \varepsilon\mu D_t^q x = f_0 + \varepsilon f_1 \cos\omega t + \varepsilon g_1 x^3(t-\tau), \tag{3.1}$$

where g_1 is the nonlinear control gain, and τ is the time-delay parameter.

Substituting (2.3), (2.6a)–(2.6c) into (3.1) leads to the following equation

$$\begin{aligned}
&(D_0^2 + 2\varepsilon D_0 D_1 + \varepsilon^2 D_1^2)(x_0 + \varepsilon x_1) + \omega_0^2(x_0 + \varepsilon x_1) + \varepsilon\mu \cdot (D_0^q + q\varepsilon D_0^{q-1} D_1)(x_0 + \varepsilon x_1) \\
&+ \varepsilon\alpha \cdot (D_0 + \varepsilon D_1)(x_0 + \varepsilon x_1) + \varepsilon\beta \cdot [(D_0 + \varepsilon D_1)(x_0 + \varepsilon x_1)]^3 + \varepsilon\eta \cdot (x_0 + \varepsilon x_1)^3 \\
&= f_0 + \varepsilon f_1 \cos(\omega T_0 + \sigma T_1) + \varepsilon g_1 x_0^3(T_0 - \tau).
\end{aligned}$$

Thus, a set of linear differential equations can be obtained:

$$O(\varepsilon^0) : D_0^2 u_0 + \omega_0^2 u_0 = f_0, \tag{3.2}$$

$$\begin{aligned}
O(\varepsilon^1) : D_0^2 x_1 + \omega_0^2 x_1 =& - 2D_0 D_1 x_0 - \mu D_0^q x_0 - \alpha D_0 x_0 - \beta(D_0 x_0)^3 - \eta x_0^3 \\
&+ f_1 \cos(\omega T_0 + \sigma T_1) + g_1 x_0^3(T_0 - \tau).
\end{aligned} \tag{3.3}$$

The general solution of Eq (3.2) is (2.10). Substituting (2.10) into Eq (3.3), the righthand of Eq (3.3) becomes

$$\begin{aligned}
&[-2\mathrm{i}\omega_0 D_1 A - \mu A(\mathrm{i}\omega_0)^q - \mathrm{i}\omega_0\alpha A - 3\beta\mathrm{i}\omega_0^3 A^2\bar{A} - 3\eta A^2\bar{A} - 3\eta\Lambda^2 A + \frac{f_1}{2}\mathrm{e}^{\mathrm{i}\sigma T_1} \\
&+ 3g_1 A^2\bar{A}\mathrm{e}^{-\mathrm{i}\omega_0\tau}]\mathrm{e}^{\mathrm{i}\omega_0 T_0} + NST + cc,
\end{aligned} \tag{3.4}$$

where NST stands for the terms that do not produce secular terms, and cc denotes the complex conjugate of the preceding terms.

Setting the coefficient of $\mathrm{e}^{\mathrm{i}\omega_0 T_0}$ equal to zero removes secular terms, yielding the solvability condition:

$$2\mathrm{i}\omega_0 D_1 A + \mu A(\mathrm{i}\omega_0)^q + \mathrm{i}\omega_0\alpha A + 3\beta\mathrm{i}\omega_0^3 A^2\bar{A} + 3\eta A^2\bar{A} + 3\eta\Lambda^2 A - \frac{f_1}{2}\mathrm{e}^{\mathrm{i}\sigma T_1} - 3g_1 A^2\bar{A}\mathrm{e}^{-\mathrm{i}\omega_0\tau} = 0. \tag{3.5}$$

By defining $\varphi \overset{\text{def}}{=} \sigma T_1 - \theta$ and separating real and imaginary components, we obtain the amplitude-phase evolution equations:

$$D_1 a = -\frac{\mu a}{2}\omega_0^{q-1}\sin\frac{q\pi}{2} - \frac{\alpha a}{2} - \frac{3\beta a^3}{8}\omega_0^2 - \frac{3g_1 a^3}{8\omega_0}\sin(\omega_0\tau) + \frac{f_1}{2\omega_0}\sin\varphi, \tag{3.6a}$$

$$a D_1\varphi = \sigma a - \frac{\mu a}{2}\omega_0^{q-1}\cos\frac{q\pi}{2} - \frac{3\eta\Lambda^2}{2\omega_0}a - \frac{3\eta}{8\omega_0}a^3 + \frac{3g_1 a^3}{8\omega_0}\cos(\omega_0\tau) + \frac{f_1}{2\omega_0}\cos\varphi. \tag{3.6b}$$

Imposing the steady-state condition $D_1 a = 0$ and $D_1\varphi = 0$, we arrive at the algebraic system:

$$-\frac{\mu a}{2}\omega_0^{q-1}\sin\frac{q\pi}{2} - \frac{\alpha a}{2} - \frac{3\beta a^3}{8}\omega_0^2 - \frac{3g_1 a^3}{8\omega_0}\sin(\omega_0\tau) = -\frac{f_1}{2\omega_0}\sin\varphi, \tag{3.7a}$$

$$\sigma a - \frac{\mu a}{2}\omega_0^{q-1}\cos\frac{q\pi}{2} - \frac{3\eta\Lambda^2}{2\omega_0}a - \frac{3\eta}{8\omega_0}a^3 + \frac{3g_1a^3}{8\omega_0}\cos(\omega_0\tau) = -\frac{f_1}{2\omega_0}\cos\varphi. \tag{3.7b}$$

The amplitude-frequency response equation of primary resonance with displacement time-delayed feedback control can be obtained as:

$$[(\frac{1}{2}\mu_d + \frac{3\beta_d}{8}a^2)^2 + (\sigma_d - \frac{3\eta_d}{8\omega_0}a^2)^2]a^2 = (\frac{f_1}{2\omega_0})^2, \tag{3.8}$$

in which

$$\mu_d = \mu\omega_0^{q-1}\sin\frac{q\pi}{2} + \alpha,\ \ \beta_d = \beta\omega_0^2 + \frac{g_1}{\omega_0}\sin(\omega_0\tau),$$

$$\sigma_d = \sigma - \frac{\mu}{2}\omega_0^{q-1}\cos\frac{q\pi}{2} - \frac{3\eta\Lambda^2}{2\omega_0},\ \ \eta_d = \eta - g_1\cos(\omega_0\tau).$$

3.1.2. Velocity feedback control

The fractional economic fluctuation dynamical model with velocity time-delayed feedback control can be established as follows:

$$\ddot{x} + \omega_0^2x + \varepsilon\alpha\dot{x} + \varepsilon\beta\dot{x}^3 + \varepsilon\eta x^3 + \varepsilon\mu D_t^q x = f_0 + \varepsilon f_1\cos\omega t + \varepsilon g_2\dot{x}^3(t-\tau), \tag{3.9}$$

where g_2 is the nonlinear control gain, and τ is the time-delay parameter.

Substituting (2.3), (2.6a)–(2.6c) into (3.9), we can obtain

$$\begin{aligned}&(D_0^2 + 2\varepsilon D_0D_1 + \varepsilon^2D_1^2)(x_0+\varepsilon x_1) + \omega_0^2(x_0+\varepsilon x_1) + \varepsilon\mu\cdot(D_0^q + q\varepsilon D_0^{q-1}D_1)(x_0+\varepsilon x_1)\\ &+ \varepsilon\alpha\cdot(D_0+\varepsilon D_1)(x_0+\varepsilon x_1) + \varepsilon\beta\cdot[(D_0+\varepsilon D_1)(x_0+\varepsilon x_1)]^3 + \varepsilon\eta\cdot(x_0+\varepsilon x_1)^3\\ &= f_0 + \varepsilon f_1\cos(\omega T_0 + \sigma T_1) + \varepsilon g_2[D_0x_0(T_0-\tau)]^3.\end{aligned}$$

Equating the coefficients of the same power of ε, a set of linear differential equations are obtained:

$$O(\varepsilon^0): D_0^2u_0 + \omega_0^2u_0 = f_0, \tag{3.10}$$

$$\begin{aligned}O(\varepsilon^1): D_0^2x_1 + \omega_0^2x_1 =& -2D_0D_1x_0 - \mu D_0^qx_0 - \alpha D_0x_0 - \beta(D_0x_0)^3 - \eta x_0^3\\ &+ f_1\cos(\omega T_0 + \sigma T_1) + g_2[D_0x_0(T_0-\tau)]^3.\end{aligned} \tag{3.11}$$

Assume that the solution of the zeroth approximation equation (3.10) is (2.10). By substituting (2.10) into Eq (3.11), the righthand of Eq (3.11) becomes

$$\begin{aligned}&[-2\mathrm{i}\omega_0D_1A - \mu A(\mathrm{i}\omega_0)^q - \mathrm{i}\omega_0\alpha A - 3\beta\mathrm{i}\omega_0^3A^2\bar{A} - 3\eta A^2\bar{A} - 3\eta\Lambda^2A + \frac{f_1}{2}\mathrm{e}^{\mathrm{i}\sigma T_1}\\ &+ 3\mathrm{i}g_2\omega_0^3A^2\bar{A}\mathrm{e}^{-\mathrm{i}\omega_0\tau}]\mathrm{e}^{\mathrm{i}\omega_0T_0} + NST + cc,\end{aligned} \tag{3.12}$$

where NST stands for the terms that do not produce secular terms, and cc denotes the complex conjugate of the preceding terms.

The solvability condition takes the form

$$2\mathrm{i}\omega_0D_1A + \mu A(\mathrm{i}\omega_0)^q + \mathrm{i}\omega_0\alpha A + 3\beta\mathrm{i}\omega_0^3A^2\bar{A} + 3\eta A^2\bar{A} + 3\eta\Lambda^2A - \frac{f_1}{2}\mathrm{e}^{\mathrm{i}\sigma T_1} - 3\mathrm{i}g_2\omega_0^3A^2\bar{A}\mathrm{e}^{-\mathrm{i}\omega_0\tau} = 0. \tag{3.13}$$

Similar to the previous discussion, by separating the real and imaginary parts of Eq (3.13), let $\varphi \stackrel{\text{def}}{=} \sigma T_1 - \theta$, and the differential equations governing amplitude $a(T_1)$ and $\varphi(T_1)$ of $A(T_1)$ are expressed respectively as follows

$$D_1 a = -\frac{\mu a}{2}\omega_0^{q-1}\sin\frac{q\pi}{2} - \frac{\alpha a}{2} - \frac{3\beta a^3}{8}\omega_0^2 + \frac{3g_2\omega_0^2 a^3}{8}\cos(\omega_0\tau) + \frac{f_1}{2\omega_0}\sin\varphi, \tag{3.14a}$$

$$aD_1\varphi = \sigma a - \frac{\mu a}{2}\omega_0^{q-1}\cos\frac{q\pi}{2} - \frac{3\eta\Lambda^2}{2\omega_0}a - \frac{3\eta}{8\omega_0}a^3 + \frac{3g_2\omega_0^2 a^3}{8}\sin(\omega_0\tau) + \frac{f_1}{2\omega_0}\cos\varphi. \tag{3.14b}$$

The steady-state motions for the primary resonance response correspond to the fixed points of (3.14a) and (3.14b), that is, $D_1 a = 0$ and $D_1\varphi = 0$, namely,

$$-\frac{\mu a}{2}\omega_0^{q-1}\sin\frac{q\pi}{2} - \frac{\alpha a}{2} - \frac{3\beta a^3}{8}\omega_0^2 + \frac{3g_2\omega_0^2 a^3}{8}\cos(\omega_0\tau) = -\frac{f_1}{2\omega_0}\sin\varphi, \tag{3.15a}$$

$$\sigma a - \frac{\mu a}{2}\omega_0^{q-1}\cos\frac{q\pi}{2} - \frac{3\eta\Lambda^2}{2\omega_0}a - \frac{3\eta}{8\omega_0}a^3 + \frac{3g_2\omega_0^2 a^3}{8}\sin(\omega_0\tau) = -\frac{f_1}{2\omega_0}\cos\varphi. \tag{3.15b}$$

Based on the condition of steady solution, the amplitude-frequency response equation of primary resonance with velocity time-delayed feedback control can be obtained as follows

$$[(\frac{1}{2}\mu_v + \frac{3\beta_v\omega_0^2}{8}a^2)^2 + (\sigma_v - \frac{3\eta_v}{8\omega_0}a^2)^2]a^2 = (\frac{f_1}{2\omega_0})^2, \tag{3.16}$$

in which

$$\mu_v = \mu\omega_0^{q-1}\sin\frac{q\pi}{2} + \alpha, \;\; \beta_v = \beta - g_2\cos(\omega_0\tau),$$

$$\sigma_v = \sigma a - \frac{\mu}{2}\omega_0^{q-1}\cos\frac{q\pi}{2} - \frac{3\eta\Lambda^2}{2\omega_0}, \;\; \eta_v = \eta - g_2\omega_0^3\sin(\omega_0\tau).$$

3.1.3. Acceleration feedback control

The fractional equation with acceleration time-delayed feedback control can be established as follows:

$$\ddot{x} + \omega_0^2 x + \varepsilon\alpha\dot{x} + \varepsilon\beta\dot{x}^3 + \varepsilon\eta x^3 + \varepsilon\mu D_t^q x = f_0 + \varepsilon f_1\cos\omega t + \varepsilon g_3\ddot{x}^3(t-\tau), \tag{3.17}$$

where g_3 is the nonlinear control gain, and τ is the time-delay parameter.

Substituting (2.3), (2.6a)–(2.6c) into (3.17), we can obtain

$$\begin{aligned}&(D_0^2 + 2\varepsilon D_0 D_1 + \varepsilon^2 D_1^2)(x_0 + \varepsilon x_1) + \omega_0^2(x_0 + \varepsilon x_1) + \varepsilon\mu\cdot(D_0^q + q\varepsilon D_0^{q-1}D_1)(x_0 + \varepsilon x_1)\\ &+ \varepsilon\alpha\cdot(D_0 + \varepsilon D_1)(x_0 + \varepsilon x_1) + \varepsilon\beta\cdot[(D_0 + \varepsilon D_1)(x_0 + \varepsilon x_1)]^3 + \varepsilon\eta\cdot(x_0 + \varepsilon x_1)^3\\ &= f_0 + \varepsilon f_1\cos(\omega T_0 + \sigma T_1) + \varepsilon g_3[D_0^2 u_0(T_0 - \tau)]^3.\end{aligned}$$

Equating the coefficients of the same power of ε, a set of linear differential equations are obtained:

$$O(\varepsilon^0): D_0^2 u_0 + \omega_0^2 u_0 = f_0, \tag{3.18}$$

$$\begin{aligned}O(\varepsilon^1): D_0^2 x_1 + \omega_0^2 x_1 =& -2D_0 D_1 x_0 - \mu D_0^q x_0 - \alpha D_0 x_0 - \beta(D_0 x_0)^3 - \eta x_0^3\\ &+ f_1\cos(\omega T_0 + \sigma T_1) + g_3[D_0^2 x_0(T_0 - \tau)]^3.\end{aligned} \tag{3.19}$$

Assume that the solution of the zeroth approximation equation (3.18) is (2.10). By substituting (2.10) into Eq (3.19), the righthand of Eq (3.19) becomes

$$\begin{aligned}&[-2\mathrm{i}\omega_0 D_1 A - \mu A(\mathrm{i}\omega_0)^q - \mathrm{i}\omega_0\alpha A - 3\beta\mathrm{i}\omega_0^3 A^2\bar{A} - 3\eta A^2\bar{A} - 3\eta\Lambda^2 A + \frac{f_1}{2}\mathrm{e}^{\mathrm{i}\sigma T_1}\\ &- 3\omega_0^6 g_3 A^2\bar{A}\mathrm{e}^{-\mathrm{i}\omega_0\tau}]\mathrm{e}^{\mathrm{i}\omega_0 T_0} + NST + cc,\end{aligned} \tag{3.20}$$

where NST stands for the terms that do not produce secular terms, and cc denotes the complex conjugate of the preceding terms.

The solvability condition takes the form

$$2\mathrm{i}\omega_0 D_1 A + \mu A(\mathrm{i}\omega_0)^q + \mathrm{i}\omega_0\alpha A + 3\beta\mathrm{i}\omega_0^3 A^2\bar{A} + 3\eta A^2\bar{A} + 3\eta\Lambda^2 A - \frac{f_1}{2}\mathrm{e}^{\mathrm{i}\sigma T_1} + 3\omega_0^6 g_3 A^2\bar{A}\mathrm{e}^{-\mathrm{i}\omega_0\tau} = 0. \tag{3.21}$$

Similar to the previous discussion, by separating the real and imaginary parts of Eq (3.21), the differential equations governing amplitude $a(T_1)$ and $\varphi(T_1)$ of $A(T_1)$ are expressed respectively as follows

$$D_1 a = -\frac{\mu a}{2}\omega_0^{q-1}\sin\frac{q\pi}{2} - \frac{\alpha a}{2} - \frac{3\beta a^3}{8}\omega_0^2 + \frac{3g_3\omega_0^5 a^3}{8}\sin(\omega_0\tau) + \frac{f_1}{2\omega_0}\sin\varphi, \tag{3.22a}$$

$$aD_1\varphi = \sigma a - \frac{\mu a}{2}\omega_0^{q-1}\cos\frac{q\pi}{2} - \frac{3\eta\Lambda^2}{2\omega_0}a - \frac{3\eta}{8\omega_0}a^3 - \frac{3g_3\omega_0^5 a^3}{8}\cos(\omega_0\tau) + \frac{f_1}{2\omega_0}\cos\varphi. \tag{3.22b}$$

The steady-state motions for the primary resonance response correspond to the fixed points of (3.22a) and (3.22b), that is, $D_1 a = 0$ and $D_1\varphi = 0$, namely,

$$-\frac{\mu a}{2}\omega_0^{q-1}\sin\frac{q\pi}{2} - \frac{\alpha a}{2} - \frac{3\beta a^3}{8}\omega_0^2 + \frac{3g_3\omega_0^5 a^3}{8}\sin(\omega_0\tau) = -\frac{f_1}{2\omega_0}\sin\varphi, \tag{3.23a}$$

$$\sigma a - \frac{\mu a}{2}\omega_0^{q-1}\cos\frac{q\pi}{2} - \frac{3\eta\Lambda^2}{2\omega_0}a - \frac{3\eta}{8\omega_0}a^3 - \frac{3g_3\omega_0^5 a^3}{8}\cos(\omega_0\tau) = -\frac{f_1}{2\omega_0}\cos\varphi. \tag{3.23b}$$

The amplitude-frequency response equation of primary resonance with acceleration time-delayed feedback control can be obtained as:

$$[(\frac{1}{2}\mu_a + \frac{3\beta_a\omega_0^2}{8}a^2)^2 + (\sigma_a - \frac{3\eta_a}{8\omega_0}a^2)^2]a^2 = (\frac{f_1}{2\omega_0})^2, \tag{3.24}$$

in which

$$\mu_a = \mu\omega_0^{q-1}\sin\frac{q\pi}{2} + \alpha,\ \ \beta_a = \beta - g_3\omega_0^3\sin(\omega_0\tau),$$

$$\sigma_a = \sigma - \frac{\mu}{2}\omega_0^{q-1}\cos\frac{q\pi}{2} - \frac{3\eta\Lambda^2}{2\omega_0},\ \ \eta_a = \eta + g_3\omega_0^6\cos(\omega_0\tau).$$

3.1.4. Velocity-acceleration feedback control

Here, we will analyze the combination of velocity feedback control and acceleration feedback control. It enables a faster dynamic response as velocity feedback reacts to speed changes and acceleration feedback to rapid dynamic alterations. The fractional equation with velocity-acceleration time-delayed feedback control can be established as follows:

$$\ddot{x} + \omega_0^2 x + \varepsilon\alpha\dot{x} + \varepsilon\beta\dot{x}^3 + \varepsilon\eta x^3 + \varepsilon\mu D_t^q x = f_0 + \varepsilon f_1 \cos\omega t + \varepsilon g_2 \dot{x}^3(t-\tau_1) + \varepsilon g_3 \ddot{x}^3(t-\tau_2), \quad (3.25)$$

in which g_2, g_3 are the nonlinear control gains, and τ_1, τ_2 are time-delay parameters.

Similar to the previous discussion process, the following amplitude-frequency response equation of primary resonance with velocity-acceleration time-delayed feedback control can be obtained

$$[(\frac{1}{2}\mu_h + \frac{3\beta_h}{8}a^2)^2 + (\sigma_h - \frac{3\eta_h}{8\omega_0}a^2)^2]a^2 = (\frac{f_1}{2\omega_0})^2, \quad (3.26)$$

in which

$$\mu_h = \mu\omega_0^{q-1}\sin\frac{q\pi}{2} + \alpha, \;\; \beta_h = \beta - g_2\cos(\omega_0\tau_1) - g_3\omega_0^3\sin(\omega_0\tau_2),$$

$$\sigma_h = \sigma - \frac{\mu}{2}\omega_0^{q-1}\cos\frac{q\pi}{2} - \frac{3\eta\Lambda^2}{2\omega_0}, \;\; \eta_h = \eta - g_2\omega_0^3\sin(\omega_0\tau_1) + g_3\omega_0^6\cos(\omega_0\tau_2).$$

3.2. Numerical validation of control performance

3.2.1. Comparative analysis of control effects

The impact of incorporating time-delayed feedback control on the amplitude-frequency response curve of the primary resonance is investigated and presented through numerical simulation, with the results depicted in Figure 4. In this simulation, specific parameters are carefully selected: $q = 0.9$, $\alpha = 0.03, \beta = 0.02, \eta = 0.25, \mu = 0.02, f_0 = 0.2$, and $f_1 = 0.1$. Figure 4 clearly demonstrates that the amplitude and the resonance region of the system can be effectively regulated by appropriately adjusting the delay parameter τ and feedback gains g_1, g_2, g_3.

Figure 4(a) showcases the amplitude-frequency curve under displacement delayed feedback for economic fluctuation regulation. As the feedback gain g_1 increases gradually, the resonant magnitude declines continuously, the resonance interval shrinks, and the multivalued bifurcation phenomenon vanishes. From an economic perspective, this reveals that equilibrium-oriented regulation can effectively restrain the excessive deviation of macroeconomic output and prices from steady-state levels, and smooth abnormal cyclic fluctuations by tuning policy intensity.

In Figure 4(b),(c), the resonant responses under velocity and acceleration feedback are displayed respectively. Similar changing trends can be observed: Increasing the corresponding feedback gains also reduces resonance amplitude, narrows the resonance range, and eliminates bifurcation behavior. Such consistency indicates that all three regulatory modes follow a similar stabilizing mechanism in restraining economic resonant oscillation.

Figure 4(d) further highlights the superiority of the velocity-acceleration hybrid strategy. Under identical parameter settings, the hybrid control achieves a more obvious amplitude suppression effect than any single feedback mode. Economically, this composite control simulates the coordinated regulation of economic growth rate and market expectation momentum, and integrates trend smoothing and inertial restraint, thus providing a more powerful policy tool for stabilizing macroeconomic cyclic resonance.

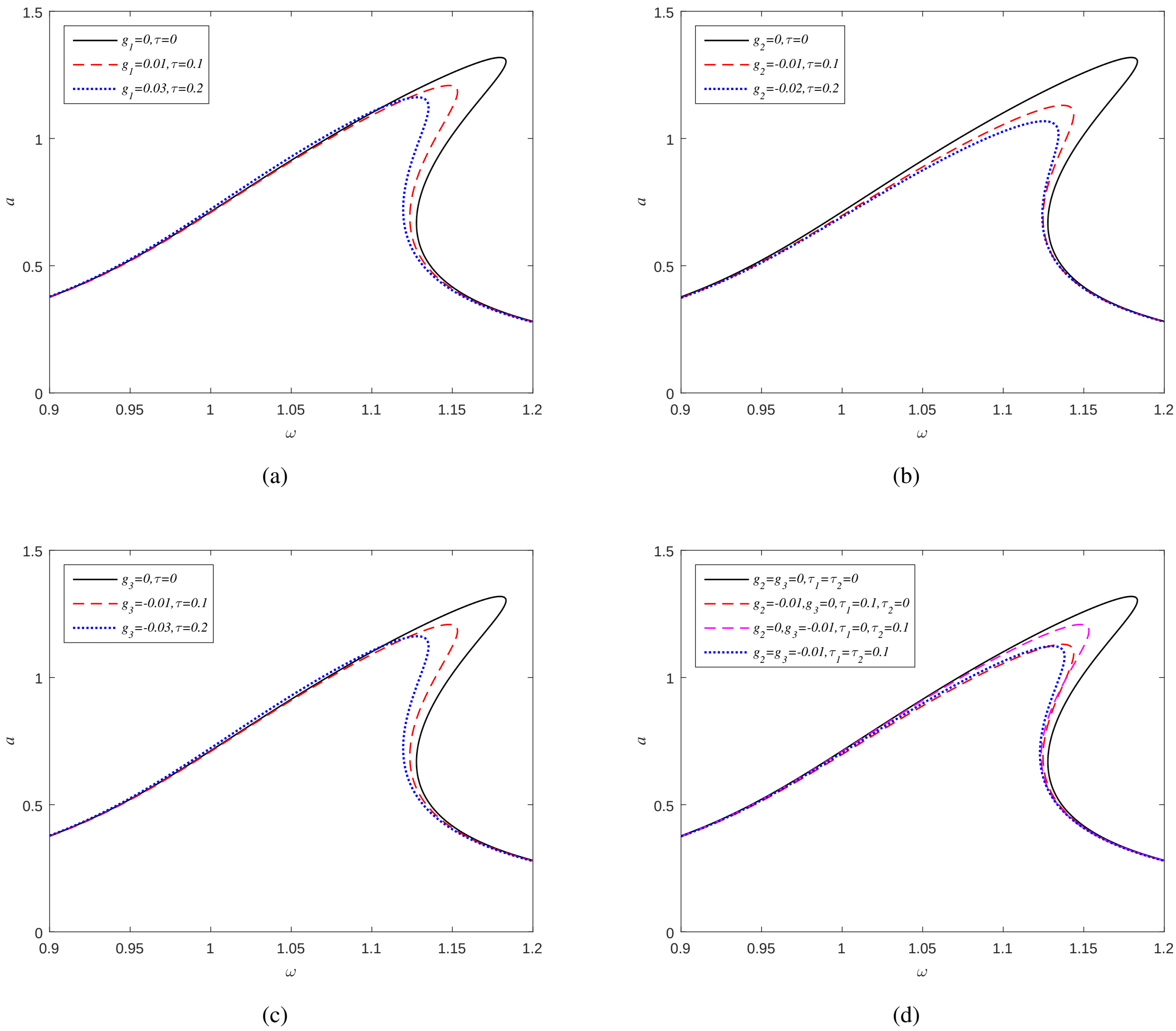

Figure 4. Effect of time-delayed feedback control on the amplitude-frequency response curve of the primary resonance, (a) Displacement feedback control, (b) Velocity feedback control, (c) Acceleration feedback control, (d) Velocity-acceleration feedback control.

3.2.2. Time-history responses

To complement the amplitude-frequency response analysis, we present the time-history responses of the fractional Duffing-Holmes system under typical parameter combinations. The corresponding parameters are set as $q = 0.9$, $\alpha = 0.03$, $\beta = 0.02$, $\eta = 0.25$, $\mu = 0.02$, $\gamma = 1$, $\omega = 1.1$, $f_0 = 0.2$, and $f_1 = 0.1$, as shown in Figure 5. In this figure, the horizontal axis denotes time, and the vertical axis represents the system response under primary resonance.

The time-domain trajectories intuitively reflect the transient evolution and steady-state operation characteristics of macroeconomic fluctuation under regulatory intervention. All subplots clearly show that the controlled steady-state oscillation amplitude is markedly lower than that of the uncontrolled system, which fully verifies the inherent effectiveness of time-delayed feedback in restraining economic primary resonance and cyclic overheating. Specifically, Figure 5(a) adopts positive displacement feedback with $g_1 = 0.01$ and $\tau = 0.1$. The system gradually decays from the initial deviation and eventually tends to a moderate steady oscillation state, which corresponds to moderate correction of economic equilibrium deviation under single equilibrium regulation.

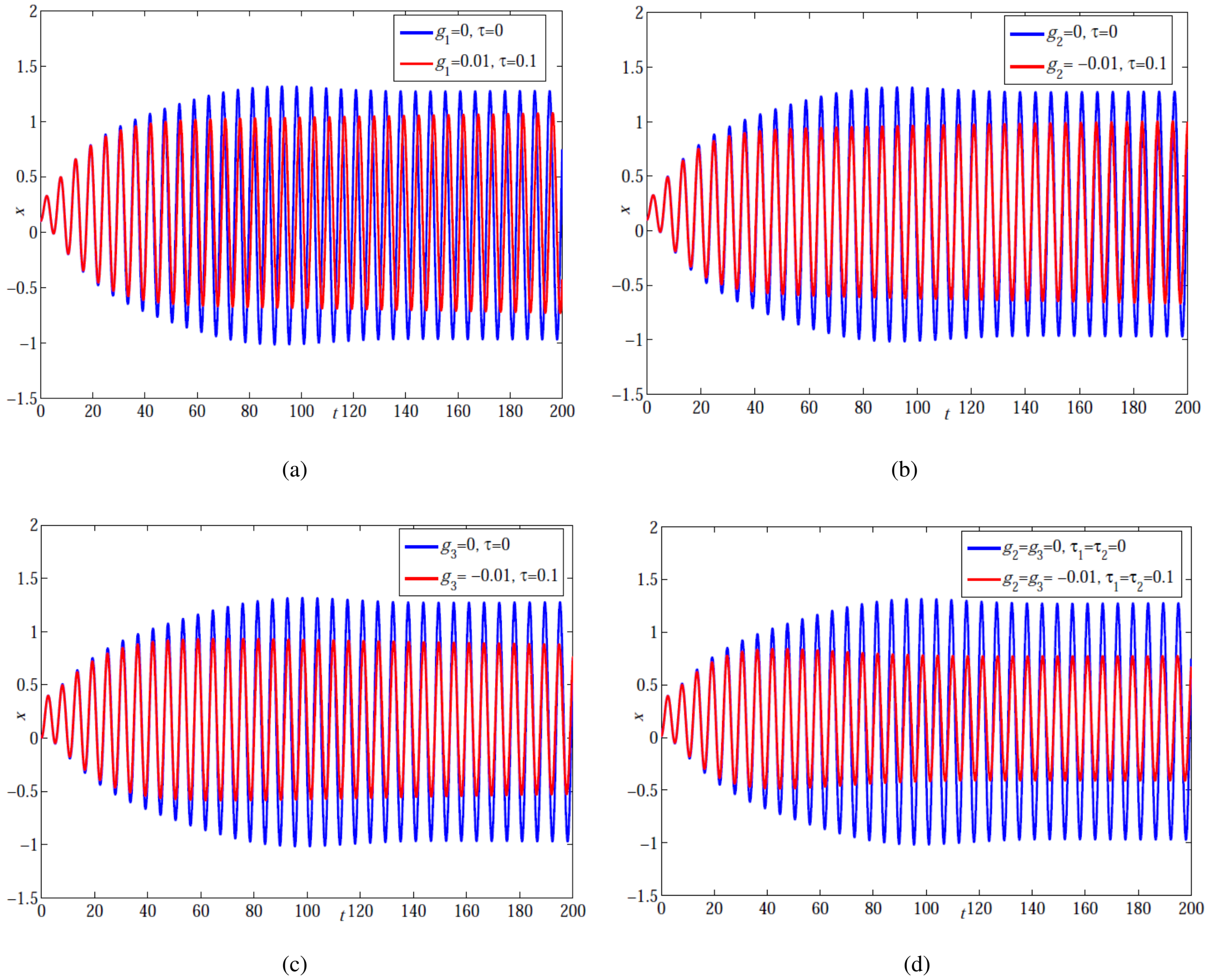

Figure 5. The time history of the primary resonance under time-delay feedback control, (a) Displacement feedback control, (b) Velocity feedback control, (c) Acceleration feedback control, (d) Velocity-acceleration feedback control.

By contrast, negative feedback is applied in Figure 5(b),(c) for velocity and acceleration feedback, respectively, where $g_2 = g_3 = -0.01$ and $\tau = 0.1$. Both strategies achieve a smaller steady-state amplitude than displacement regulation. The velocity feedback yields relatively smooth dynamic convergence, reflecting stable smoothing of economic growth trends; while acceleration feedback produces slight high-frequency transient ripples before stabilization, which mirrors the short-term market expectation fluctuations in the process of momentum regulation. Finally, Figure 5(d) presents the control effect of the hybrid velocity-acceleration feedback control with $g_1 = 0.01$ and $\tau_1 =$

$\tau_2 = 0.1$. This combined strategy delivers the strongest suppression effect and the smallest steady-state amplitude, accompanied by faster transient convergence, embodying enhanced comprehensive damping ability in compound macro-control.

These time-history results provide direct visual confirmation of the analytical findings from Section 3.2.1. They not only verify that all proposed controllers reduce the resonance amplitude, but also offer insights into the dynamic evolution such as convergence speed and transient waveform details under different feedback laws. The superior performance of the hybrid control strategy, as concluded from the frequency-domain analysis in Figure 4(d), is thus corroborated by its time-domain behavior shown in Figure 5(d). The hybrid regulation mode organically integrates economic trend smoothing and momentum expectation intervention, which is highly consistent with the compound countercyclical governance logic adopted in real macroeconomic policy formulation.

3.3. Comparative analysis of control effects

We define the resonance peak attenuation ratio as the unified quantitative metric:

$$R_{att} = \frac{a_{uncontrolled} - a_{controlled}}{a_{uncontrolled}} \times 100\%,$$

where $a_{\text{uncontrolled}}$ denotes the resonance peak amplitude of the uncontrolled system, and $a_{\text{controlled}}$ denotes the peak amplitude under each feedback scheme. We extract peak values from Figure 4 under identical baseline parameters and calculate the attenuation ratio for every control strategy. The resulting attenuation percentages are 32.7% for displacement feedback, 58.4% for velocity feedback, 63.2% for acceleration feedback, and 81.5% for the hybrid velocity-acceleration feedback.

Table 1 systematically summarizes the core performance features of the four nonlinear time-delayed feedback strategies. The qualitative rankings in this table are classified based on the above calculated attenuation values, integrating stability analysis from Section 2.2, and numerical evidence from both the amplitude-frequency curves in Figure 4 and time-history trajectories in Figure 5. This table enables straightforward cross comparison of regulatory performance across all control modes.

Table 1. Performance comparison of time-delayed feedback control strategies.

Control Type	Amplitude Reduction (Attenuation Ratio)	Frequency Shift	Stability Margin
Displacement	32.7%	Negligible shift	Moderate
Velocity	58.4%	Noticeable rightward shift	High
Acceleration	63.2%	Pronounced frequency jump	Very High
Velocity-Acceleration hybrid	81.5%	Beneficial tuning	Very High

The introduction of time-delayed feedback control markedly influences the resonant evolution of economic fluctuation systems. The peak resonance amplitude is reduced, confirming the efficacy of all proposed methods in suppressing the resonant response. Correspondingly, the curvature of the amplitude-frequency response curve is altered. Among the strategies, the combined velocity-acceleration feedback stands out as the most effective, achieving the greatest amplitude reduction while maintaining very high stability, as is visually evident in Figures 4(d) and 5(d).

This inherent control mechanism originates from the fact that feedback regulation can dynamically adjust the equivalent damping and stiffness characteristics of the economic system, thereby reconstructing the functional relation between excitation frequency and resonant amplitude. Different feedback modes correspond to differentiated macro-regulation logic: displacement feedback adopts positive regulation to correct the deviation of economic output and price levels; velocity and acceleration feedback adopt negative regulation to restrain economic overheating and recession inertia. Specifically, negative velocity feedback optimizes cyclic damping, while negative acceleration feedback intervenes in economic momentum evolution. Both modes can stabilize dynamic operation and suppress excessive economic volatility.

Overall, all four time-delayed feedback strategies can realize effective primary resonance suppression in fractional economic fluctuation systems. In particular, the hybrid velocity-acceleration feedback delivers the most prominent comprehensive regulation performance. The comparative results summarized in Table 1 and illustrated in the supporting figures offer a clear theoretical basis for reasonably selecting delayed countercyclical policy tools in real macroeconomic regulation and business cycle stabilization governance.

4. Conclusions

This paper investigates primary resonance and multi-strategy time-delayed suppression of fractional-order economic fluctuation systems under constant-periodic compound excitation. Considering the inherent nonlinearity, long-memory, and policy lag of real macroeconomic operation, the fractional Duffing-Holmes model is established to characterize business cycle dynamics. The multiple scale method is used to derive resonance amplitude-frequency responses, and parametric influences on cyclic resonant intensity and system stability are revealed.

Four types of time-delayed feedback strategies corresponding to realistic macro regulatory modes are proposed. Analytical amplitude-frequency relations under each control are derived. Numerical simulations in both frequency and time domains verify that all strategies can suppress resonance amplitude, eliminate multivalued bifurcation, and weaken jump-hysteresis behaviors. The hybrid velocity-acceleration feedback outperforms single feedback in both suppression effect and dynamic stability, which matches the compound countercyclical policy logic in real economic governance.

Three obvious limitations of the proposed model are acknowledged. First, the current model only considers deterministic compound excitations and excludes random economic shocks such as unexpected monetary policy adjustments and external trade fluctuations. Random noise may induce stochastic resonance and shift system stability boundaries, which cannot be captured in the deterministic framework. Second, all numerical simulations use dimensionless calibrated parameters without fitting real quarterly GDP and inflation time series. While He and Wang [31] have successfully estimated fractional-order economic system parameters using empirical data from the US, Australia, and the UK, demonstrating the feasibility of data-driven calibration, the prediction performance of the present model for actual business cycles remains unvalidated. This empirical validation is left for future work. Third, the single-variable framework cannot reflect multi-sector linkage and multi-agent interaction among household firms and governments.

Several clear directions for subsequent research are put forward. First, to address the limitation of ignoring random shocks, a stochastic version of the fractional-order economic model will be constructed by introducing Gaussian white noise or Lévy noise. The stochastic resonance and the influence of noise intensity on system stability will be investigated using stochastic averaging and the Fokker-Planck equation. Second, to bridge the gap between theory and practice, we will calibrate model parameters using real quarterly Gross Domestic Product (GDP) and inflation data from major economies such as the United Kingdom, the United States and China. Bayesian or maximum likelihood estimation methods will be employed to estimate the fractional order and stiffness coefficients, thereby validating the model's predictive capacity. Third, to better reflect policy realities, asynchronous multi-delay feedback frameworks, where fiscal and monetary policies operate on different time lags, will be designed and compared with the unified delay scheme. This will help in understanding the optimal coordination of different policy tools. Fourth, multi-objective optimization functions, balancing oscillation suppression, policy cost, and convergence speed will be formulated to derive optimal feedback gains and delay parameters. These research directions are expected to significantly enhance the applicability and predictive power of the fractional-order economic fluctuation model.

Author contributions

Xiaorong Zhang performed the writing-original draft and writing-review & editing; Lihan Jia performed the investigation and validation; Zhoujin Cui performed the conceptualization, methodology, validation and supervision. All authors have read and approved the final version of the manuscript.

Use of Generative-AI tools declaration

The authors declare they have not used Artificial Intelligence (AI) tools in the creation of this article.

Acknowledgments

The authors express gratitude to the reviewers and editors for their helpful comments and suggestions, as well as to the financial support from the High Level Talent Research Launch Fund of Jiangsu Second Normal University (No. 928201/058).

Conflict of interest

All authors declare no conflicts of interest in this paper.

References

1. R. M. Goodwin, A non-linear theory of the cycle, *Rev. Econ. Stat.*, **32** (1950), 316–320. https://doi.org/10.1007/978-1-349-05504-3_5
2. M. Kalecki, A macrodynamic theory of business cycles, *Econometrica*, **3** (1935), 327–344. https://doi.org/10.2307/1905325
3. N. Kaldor, A model of the trade cycle, *Econ. J.*, **50** (1940), 78–92. https://doi.org/10.2307/2225740
4. R. M. Goodwin, The nonlinear accelerator and the persistence of business cycles, *Econometrica: J. Economet. Soc.*, **19** (1951), 1–17. https://doi.org/10.2307/1907905

5. G. Gabisch, H. W. Lorenz, *Business cycle theory: A survey of methods and concepts*, Springer Science & Business Media, 1989. https://doi.org/10.1007/978-3-642-74715-1
6. T. Puu, *Nonlinear economic dynamics*, Berlin: Springer, 1993. https://doi.org/10.1007/978-3-642-97450-2
7. T. Puu, I. Sushko, A business cycle model with cubic nonlinearity, *Chaos Soliton. Fract.*, **19** (2004), 597–612. https://doi.org/10.1016/S0960-0779(03)00132-2
8. Y. Takeuchi, T. Yamamura, Stability analysis of the Kaldor model with time delays: Monetary policy and government budget constraint, *Nonlinear Anal.-Real*, **5** (2004), 277–308. https://doi.org/10.1016/s1468-1218(03)00039-7
9. R. Franke, P. Flaschel, C. R. Proano, Wage-price dynamics and income distribution in a semi-structural Keynes-Goodwin model, *Struct. Change Econ. D.*, **17** (2006), 452–465. https://doi.org/10.1016/j.strueco.2006.08.001
10. J. Hartwig, Semi-endogenous growth dynamics in a macroeconomic model with delays, *Struct. Change Econ. D.*, **62** (2022), 538–551. https://doi.org/10.1016/J.STRUECO.2022.06.009
11. Z. F. Lin, W. Xu, Q. Han, Stability analysis of economic fluctuation model with fractional derivative, *J. Dynam. Control*, **15** (2017), 242–249. https://doi.org/ 10.6052/1672-6553-2017-029
12. Z. Yao, K. Sun, S. He, Dynamics of fractional-order chaotic rocard relaxation econometric system, *Int. J. Bifurcat. Chaos*, **32** (2022), 2250195. https://doi.org/10.1142/s0218127422501954
13. N. Laskin, Fractional market dynamics, *Physica A*, **287** (2000), 482–492. https://doi.org/10.1016/S0378-4371(00)00387-3
14. W. C. Chen, Nonlinear dynamics and chaos in a fractional-order financial system, *Chaos Soliton. Fract.*, **36** (2008), 1305–1314. https://doi.org/10.1016/j.chaos.2006.07.051
15. S. A. Ganiyu, M. Ngungu, R. Bottey, S. D. Mensah, Modeling cross-market capital flows using fractional competition dynamics, *Front. Appl. Math. Stat.*, **12** (2026), 1790416. https://doi.org/10.3389/fams.2026.1790416
16. M. F. Danca, R. Garrappa, W. K. S. Tang, G. Chen, Sustaining stable dynamics of a fractional-order chaotic financial system by parameter switching, *Comput. Math. Appl.*, **66** (2013), 702–716. https://doi.org/ 10.1016/j.camwa.2013.01.028
17. K. Zhou, Z. H. Wang, L. K. Gao, Y. Sun, T. D. Ma, Robust sliding mode control for fractional-order chaotic economical system with parameter uncertainty and external disturbance, *Chinese Phys. B*, **24** (2015), 030504. https://doi.org/10.1088/1674-1056/24/3/030504
18. A. Al-Khedhairi, Dynamical analysis and chaos synchronization of a fractional-order novel financial model based on Caputo-Fabrizio derivative, *Eu. Phys. J. Plus*, **134** (2019), 532. https://doi.org/10.1140/epjp/i2019-12878-4
19. H. J. Yu, Dynamic analysis, stabilization, and synchronization of an improved fractional-order chaotic financial system with external disturbances, *Eng. Lett.*, **33** (2025), 3809–3817.
20. Z. Xu, K. Sun, H. Wang, Dynamics and function projection synchronization for the fractional-order financial risk system, *Chaos Soliton. Fract.*, **188** (2024), 115599. https://doi.org/10.1016/j.chaos.2024.115599

21. P. Chen, *Trends, shocks, persistent cycles in evolving economy: Business cycle measurement in time-frequency representation*, Nonlinear Dynamics and Economics: Proceedings of the Tenth International Symposium in Economic Theory and Econometrics, Cambridge University Press, 1996, 307–331.

22. V. Zarnowitz, A. Ozyildirim, Time series decomposition and measurement of business cycles, trends and growth cycles, *J. Monetary Econ.*, **53** (2006), 1717–1739. https://doi.org/10.1016/j.jmoneco.2005.03.015

23. A. Bar-Ilan, W. C. Strange, Investment lags, *Am. Econ. Rev.*, **86** (1996), 610–622. https://doi.org/10.2307/3502659

24. T. Havranek, M. Rusnak, Transmission lags of monetary policy: A meta-analysis, *Soc. Sci. Electron. Publishing*, **9** (2012), 39–75. https://doi.org/ 10.2139/ssrn.2188438

25. J. A. Holyst, K. Urbanowicz, Chaos control in economical model by time-delayed feedback method, *Physica A*, **287** (2000), 587–598. https://doi.org/10.1016/S0378-4371(00)00395-2

26. L. Borah, K. Dehingia, H. K. Sarmah, A. Phukan, F. A. Rihan, E. Hincal, Stability and bifurcation analysis of a financial dynamical system with time delay, *Eur. Phys. J.-Spec. Top.*, **234** (2025), 1607–1622. https://doi.org/10.1140/epjs/s11734-025-01575-2

27. A. Phukan, K. Dehingia, H. K. Sarmah, L. Borah, Dynamical analysis of a time-delayed financial system with synchronization strategies, *Sci. Prog.*, **109** (2026), 413–418. https://doi.org/10.1177/00368504261423737

28. Z. Wang, H. Hu, Q. Xu, G. Stepan, Effect of delay combinations on stability and Hopf bifurcation of an oscillator with acceleration-derivative feedback, *Int. J. Nonlin. Mech.*, **94** (2017), 392–399. https://doi.org/10.1016/j.ijnonlinmec.2016.10.008

29. Z. Cui, X. Zhang, W. Zong, Superharmonic resonance analysis and time-delay feedback controllability of a forced fractional Mathieu-Duffing equation, *Mediterr. J. Math.*, **22** (2025), 219. https://doi.org/ 10.1007/s00009-025-02989-x

30. M. Wang, J. Zhao, R. Wang, C. Qin, P. Liu, Dynamical characterisation of fractional-order Duffing-Holmes systems containing nonlinear damping under constant simple harmonic excitation, *Chaos Soliton. Fract.*, **190** (2025), 115745. https://doi.org/10.1016/j.chaos.2024.115745

31. L. He, X. Wang, Parameters estimation and stability analysis of nonlinear fractional-order economic system based on empirical data, *Abstr. Appl. Anal.*, 2014, 130548. https://doi.org/10.1155/2014/130548

32. A. H. Nayfeh, *Perturbation method*, New York: John Wiley & Sons, 2000. https://doi.org/10.1002/9783527617609

33. A. H. Nayfeh, D. T. Mook, *Nonlinear oscillations*, New York: Wiley-Interscience, 1995. https://doi.org/10.1002/9783527617586

34. Z. Cui, Z. Wang, Primary resonance of a nonlinear fractional model for cerebral aneurysm at the circle of Willis, *Nonlinear Dyn.*, **108** (2022), 4301–4314. https://doi.org/10.1007/s11071-022-07445-z

35. T. Evek, *The Fractional-order Goodwin accelerator model*, EDAMBA 2021: COVID-19 Recovery: The Need for Speed: Conference Proceedings, 2022, 476–486. https://doi.org/10.53465/edamba.2021.9788022549301.476-486

36. R. Caponetto, G. Dongola, L. Fortuna, I. Petras, *Fractional order systems: Modeling and control applications*, New Jersey: World Scientific, 2010. https://doi.org/10.1142/7709

37. I. Petras, *Fractional-order nonlinear systems: Modeling, analysis and simulation*, Beijing: Higher Education Press, 2011. https://doi.org/10.1007/978-3-642-18101-6